Biosensors and Bioelectronics ■ (■■■■) ■■■–■■■

Contents lists available at ScienceDirect

Biosensors and Bioelectronics

journal homepage: www.elsevier.com/locate/bios

One step biofunctionalized electrospun multiwalled carbon nanotubes embedded zinc oxide nanowire interface for highly sensitive detection of carcinoma antigen-125

K. Brince Paul [a], Vikrant Singh [b], Siva Rama Krishna Vanjari [a], Shiv Govind Singh [a,*]

[a] Department of Electrical Engineering, Indian Institute of Technology, Hyderabad, India
[b] School of Medicine, University of California Davis, USA

ARTICLE INFO

Article history:
Received 23 May 2016
Received in revised form
20 July 2016
Accepted 31 July 2016

Keywords:
Ultrasensitive
Multiwalled carbon nanotubes
Electrospinning
Carcinoma antigen
Immunosensor

ABSTRACT

Ovarian cancer is the most leading cause of cancer-related death in women . The carcinoma antigen-125, which is found on the surface of many ovarian cancer cells is known to be a gold standard clinical biomarker associated with life-threatening gynecological malignancy. In this work, we demonstrate a novel biosensor platform based on multiwalled carbon nanotubes embedded zinc oxide nanowire for the ultrasensitive detection of carcinoma antigen-125. Label free detection of the carcinoma antigen-125 was accomplished by differential voltammetry technique that demonstrated excellent sensitivity (90.14 μA/(U/mL)/cm^2) with a detection limit of 0.00113 UmL^{-1} concentration. The fabricated immunosensor exhibits good performance with wider detection range (0.001 UmL^{-1}–1 kUmL^{-1}), reproducibility, selectivity, acceptable stability, and thus is a potential cost-effective methodology for point-of-care diagnosis. The multiwalled carbon nanotubes (MWCNTs) embedded highly oriented zinc oxide (ZnO) nanowires were synthesized by simple, low cost electrospinning technique. Compared to pure ZnO nanowires, electrochemical activity of MWCNTs embedded ZnO nanowires was found to be much higher. The calcination temperature was optimized to avoid any decomposition of the CNTs and to obtain multiwalled carbon nanotubes embedded highly crystalline ZnO nanowires. The salient feature of this biosensing platform is that one step calcination process is enough to create the functional groups on MWCNT-ZnO nanowire surface that are effective for the covalent conjugation of antibody without further surface modification. To the best of our knowledge, this is the first report on MWCNT-ZnO nanowire based immunosensor explored for the detection of cancer biomarker.

1. Introduction

Ovarian cancer is the most frequent cause in cancer associated deaths in women (Badgwell and Bast Jr., 2007). Inability to detect it in early stages leads to a dismal 5-year survival rate of 11% (Morice et al., 2003). Therefore, developing methods for early stage diagnosis of ovarian cancer is critical to ensure long term survival. Carcinoma antigen-125 (CA125) also known as mucin 16 or MUC16, a member of mucin family of glycoproteins, is found on the surface of many ovarian cancer cells. CA125 is the most used clinical biomarker for ovarian cancer (Nustad et al., 1996 ; Peng et al., 2011). The CA125 assays can be used as a screening test for the early detection of ovarian cancer, distinguish between benign and malignant disease and to monitor progress of patients with ovarian cancer (Felder et al., 2014). Current analytical methods of CA 125 levels measurements are based on radiometric or immunoassay techniques (McQuarrie et al., 1997; Wu et al., 2007a). These assays, in general, are time-consuming, costly and require skilled man power. The application of metal oxide nanostructured material has gained much popularity for highly sensitive and selective development of point of care diagnostic devices (Singh et al., 2015). In this endeavor, there is a good scope to develop the immunosensor based on the metal oxide nanobiosensor platform for the early detection of cancer biomarkers (Liu, 2008).

One dimensional (1D) metal oxides have found interesting applications in point of care diagnostic devices due to the inherent advantages of nanoregime such as high thermal, chemical and mechanical stability (Ding et al., 2010; Hsu et al., 2012; Matlock-Colangelo and Baeumner, 2012). They can provide faster electron transport as compared to the bulk (Lee et al., 2009). Among them, zinc oxide has proved to be a promising template because of its unique properties such as high surface to volume ratio, high electron transfer capability, biocompatibility and high isoelectric point of about 9.5 (Ahmad et al., 2010a, 2010b). Owing to the

* Corresponding author.
E-mail address: sgsingh@iith.ac.in (S.G. Singh).

http://dx.doi.org/10.1016/j.bios.2016.07.114
0956-5663/

higher diffusion coefficient and electron mobility of ZnO and one dimensional (1D) ZnO nanostructures are well suited for the development of electrochemical biosensors (Ali et al., 2015; Tak et al., 2014; Vasudev et al., 2013; Wei et al., 2010b). However high resistivity of ZnO and requirement for additional surface modification for immobilization of biomolecules are major limitations that needs attention while developing high sensitivity biosensors (Paul et al., 2016). To overcome these limitations, a general way is to dope ZnO nanostructures with suitable material which can tune the band gap of ZnO thereby enhancing the sensing properties by providing better conducting path (Wei et al., 2010a; Zhao et al., 2011, 2007).

Recently, multiwalled carbon nanotubes (MWCNTs) attracted much attention due to their excellent electrical conduction for enhanced bio-electrochemical reactions and significant surface area which enables carbon nanotubes as a promising material for immobilization of proteins (Odaci et al., 2008). Furthermore, highly sensitive biosensors can be developed by grafting CNTs in to metal oxide nanostructures (Gooding, 2005; Liu et al., 2012). Doping of ZnO with MWCNTs or ZnO-MWCNT hybrid nanostructures exhibit enhanced sensing performance compared to MWCNT or ZnO alone (Khanderi et al., 2009; Samadi et al., 2012). There are some reports in literature on ZnO-MWCNT nanostructures for sensing applications (Haghighi and Bozorgzadeh, 2011; Wang et al., 2011; Palanisamy et al., 2012; Fang et al., 2009; Zhang et al., 2010a; Tak et al., 2013). However, to the best of our knowledge, there is no previous report on the application of MWCNT doped ZnO or MWCNT-ZnO hybrid nanofiber based immunosensor that is developed utilizing simple, robust, well explored, low cost electrospinning technique. Nanofiber synthesized by electrospinning method have high surface to volume ratio and possess good mechanical and physical properties, they can easily be doped with suitable elements (Batra et al., 2015; Zhang et al., 2011; Zhang et al., 2010b). A few reports on the study of CA 125 detection based on quantum dots, nanoparticle, nanocomposite and molecular imprinting method (Chen et al., 2008; Johari-Ahar et al., 2015; Ravalli et al., 2013; Viswanathan et al., 2012; Wu et al., 2007b) suffer from the limitations of additional surface modification requirements for protein conjugation and signal amplification. These can be addressed by a novel MWCNT-ZnO nanofiber immunosensor synthesized via electrospinning method.

In the present work, we have demonstrated ultrasensitive MWCNT-ZnO electrochemical biosensor platform utilizing electrospinning technique which combines the unique properties of both ZnO and MWCNTs. A remarkably simple, single step functionalization of the nanofiber was developed for immobilization of anti-CA-125 antibody. It was used for the direct detection of CA125 via antigen–antibody interaction. Differential pulse voltammetry (DPV) is used as transduction mechanism as it is one of the efficient techniques for analyzing CA125 antigen-antibody interaction kinetics. To the best of our knowledge, this is the first report on ZnO-MWCNT nanofiber based immunosensor explored for direct detection of CA 125 antigen.

2. Materials and methods

2.1. Chemicals and Reagents

Carcinoma Antigen 125 protein (4.2 mg per mL) from human cell and monoclonal CA 125 antibody (366 kU per mL) raised in mouse were purchased from Fitzgerald, USA. Zinc acetate dihydrate ($Zn(CH_3COO)_2$ 2H2O,99%), Polyacrylonitrile (PAN, MW = 150,000), N,N dimethylformamide(DMF), Phosphate Buffer Saline (PBS, pH 7.4) tablets, N-hydroxysuccinimide (NHS), N-ethyl-N0-(3-dimethylaminopropyl carbodiimide) (EDC), Bovine serum albumin (BSA), Biotin–hydrazide and streptavidin, were procured from Sigma-Aldrich, USA. Pristine MWCNT (diameter: 20–70 nm and length: 1–10 μm) was obtained from Reinste Nano Ventures. Creatinine protein and immunoglobulin G (IgG) were obtained from abcam, India. Histidine-rich protein II (HRP2) was obtained from Fitzgerald, USA.

Phosphate Buffer Saline (PBS, 10 mM, pH 7.4) was prepared by dissolving PBS tablets (pH 7.4) in 200 mL deionized water obtained from Millipore water purification systems (resistivity 18.2 MΩ cm). The carboxylic acid linker solution containing 0.4 M EDC and 0.1 M NHS was prepared in 10 mM PBS buffer solution (pH 7.4). Phosphate Buffer pH 7.4 was used for anti-CA 125 antibody dilution and preparing the different concentration of carcinoma antigen-125 (CA125). The human serum samples obtained from the hospital were diluted (dilution 1/1000) in 10 mM PBS buffer solution pH 7.4.

2.2. Synthesis of CNT incorporated ZnO nanofibers (MZnONF)

MWCNT-ZNO nanofibers were synthesized by electrospinning method and followed by calcination of nanofibers at optimized temperature. In a typical experiment, a known quantity of MWCNTs were dispersed in DMF by ultrasonication for 15 min to form a black slurry followed by addition of 8 wt% of PAN. The mixture was stirred for 2 h at 65 °C. Then 4 wt% of Zinc acetate dehydrate was added to the above solution and the stirring was continued for another 3 h at about 60 °C to obtain the desired homogeneous precursor solution The maximum percentage of MWCNTs that can be added to obtain uniform nanofibers was optimized to be 4 wt%. Beyond this percentage, adverse effects of electrostatic repulsion and segregation at the grain boundaries were observed. Weight percentages of zinc acetate and PAN were also optimized to get a uniform bead free fiber. For comparison, pure ZnO nanofibers were synthesized by following exactly same procedure with the polymer precursor solution devoid of MWCNTs. For electrospinning, the prepared precursor solution was loaded into 5 mL syringe with 26 gauge metallic needles. The electrospinning process was conducted using an electric field of about 2 kV/cm applied in between needle tip and silicon substrate ground at a flowrate (40 μL/min) adjusted to yield a stable Taylor cone. The thick free standing mat of non-woven fibers were collected after 3 h of electrospinning. The formed nanofiber mats were calcined in air at different temperature for 2 h (heating rate: 5 °C min^{-1}). At higher calcination temperatures the decomposition of MWCNT was observed. Thus, the critical calcination temperature was optimized to ensure the presence of CNT with the decomposition of PAN to obtain uniform CNT-ZnO nanofiber. Interestingly, oxidizing the CNT at higher temperature creates functional groups at the surface which can be utilized for direct immobilization of protein molecules without further surface modification.

2.3. Fabrication of the MZnONF/GCE electrodes

The Glassy carbon (GCE, φ = 3 mm) working electrodes were well polished with 0.05 μm alumina slurry on a microcloth polishing pad to obtain a mirror finish and then cleaned in deionized water. After being dried at a room temperature, 6 μL of MZnONF suspension was dropped on the cleaned GCE to obtain nanofiber modified electrode (MZnONF/GCE). The modified electrodes were then washed thoroughly with deionized water to remove unbound nanofibers off the electrodes surface and the electrodes were allowed to dry at controlled room temperature ambience. The casting suspension was prepared by dispersing MWCNT-ZnO (MZnONF) nanofiber mat in DMF (0.5 mg/mL) followed by ultrasonication for 1 h. For comparison, Zinc Oxide nanofiber modified

Please cite this article as: Paul, K.B., et al., (2016), http://dx.doi.org/10.1016/j.bios.2016.07.114

electrodes (ZnO/GCE) were also prepared using the same procedure.

2.4. Immobilization of anti-CA125 antibodies on to the MZnONF/GCE electrodes

Prior to antibody immobilization, the fabricated MZnONF/GCE electrodes were treated with EDC-NHS crosslinking solution for 4 h to activate –COOH functional groups available on the MZnONF nanofiber surface. The linker solution containing 0.4 M EDC (coupling agent) and 0.1 M NHS (activator) was prepared in PBS buffer solution (10 mM, pH 7.4). After washing with PBS (pH 7.0), 6 μL of anti-CA125 antibody (200 μg/mL, prepared in PBS pH 7.4) was dropped on to the MZnONF/GCE electrode surface and incubated at 4 °C overnight. The antibodies were covalently attached to the MZnONF nanofiber surface via strong amide bonds(C–N) formed between the $–NH_2$ groups of anti-Ca125 and activated –COOH groups of MZnONF nanofiber. Thereafter, the antibody modified immunoelectrode (Anti-CA125/MZnONF/GCE) was thoroughly washed with PBS (pH 7.0) three times to remove any unbound antibodies from the electrode surface . Further, 6 μL of BSA(1%) solution was dropped on to the electrode surface and incubated for 1 h at 37 °C to eliminate the non-specific binding sites of Anti-CA125/MZnONF/GCE immunoelectrode. Finally, the fabricated BSA/Anti-CA125/MZnONF/GCE immunoelectrode was washed with PBS (pH 7.0) to remove any unbound BSA and stored at 4 °C until further use. Prior to electrochemical measurements, the modified immune electrodes were rinsed gently with de-ionized water to remove PBS from the electrode surface. Before employing the cancer detection, the performance of the MZnONF/GCE immunosensor was verified with standard Biotin-Streptavidin interaction as model system using the exactly same procedure that was used to prepare the BSA/Anti-CA125/MZnONF/GCE immunosensor. The stepwise fabrication process of the BSA/Anti-CA125/MZnONF/GCE immunosensor is shown in Scheme 1.

2.5. Electrochemical measurements

All electrochemical measurements were performed using an electrochemical analyzer CHI660E (CH Instruments, TX, USA) in 0.01 M phosphate buffer saline (PBS, pH 7.4) containing 5 mM $[Fe(CN)_6]^{3-/4-}$ as redox probe. Cyclic Voltammetry (CV, potential range from −0.4 to 0.8 V at 50 mV/s) and Differential Pulse Voltammetry (DPV, potential sweep from −0.4 to 0.6 with 0.05 V amplitude) techniques were utilized to characterize the stepwise fabrication of the immunoelectrode. The electrochemical response of immunoelectrodes (BSA/Anti-CA125/MZnONF/GCE) have been conducted as a function of carcinoma antigen-125 concentration varying from 0.001 UmL^{-1} to 1 $kUmL^{-1}$ in PBS (0.01 M, pH 7.4) containing 5 mM $[Fe(CN)_6]^{3-/4-}$ with optimized incubation time of about thirty minutes. The real sample analysis of immunosensors were evaluated by spiking different concentrations of carcinoma antigen −125 in to diluted human serum samples and the recoveries of different concentration of carcinoma antigen −125 in diluted serum were calculated from the related calibration graph (dilution ratio included). The interference studies of immunoelectrode have been carried out in presence of carcinoma antigen −125(10 UmL^{-1}) with various interferents such as, immunoglobulin G (IgG, 10 ng/mL), bovine serum albumin (BSA, 10 ng/mL), histidine-rich protein II (HRP2,10 ng/mL), creatinine (10 ng/mL) and mixture of all.

3. Results and discussions

3.1. Morphological and Structural characterization

The surface morphology of synthesized nanofibers was confirmed by the field emission-scanning electron microscopy (FE-SEM) and Transmission electron microscopy (TEM) studies. FE-SEM images of as-spun polyacrylonitrile-Zinc Acetate (PAN/ZnAc) and MWCNT- polyacrylonitrile-Zinc Acetate (MWCNT/PAN/ZnAc) nanofibers synthesized using electrospinning technique before calcination are shown in Fig. 1a and b respectively. The electrospinning parameters such as flowrate, distance and voltage were optimized to obtain uniform polymeric fibers with diameters in the range of 300–400 nm. Concentrations of PAN and ZnAc were also optimized to produce a uniform diameter, bead free continuous fiber mat. Maximum doping concentration of MWCNT was

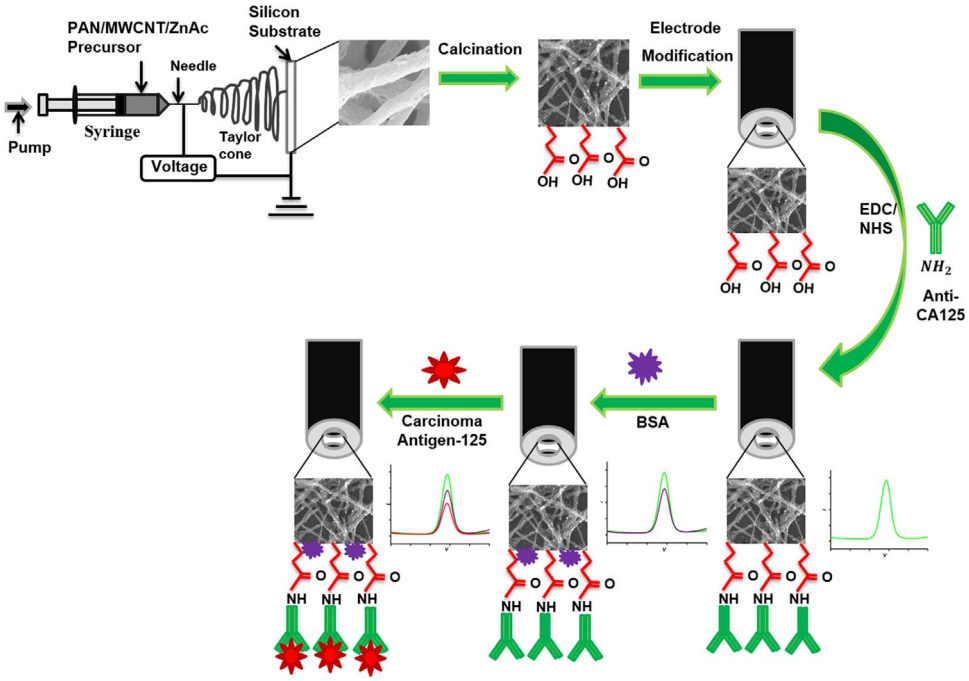

Scheme 1. Schematic representation of the fabrication of carcinoma antigen-125 immunosensor.

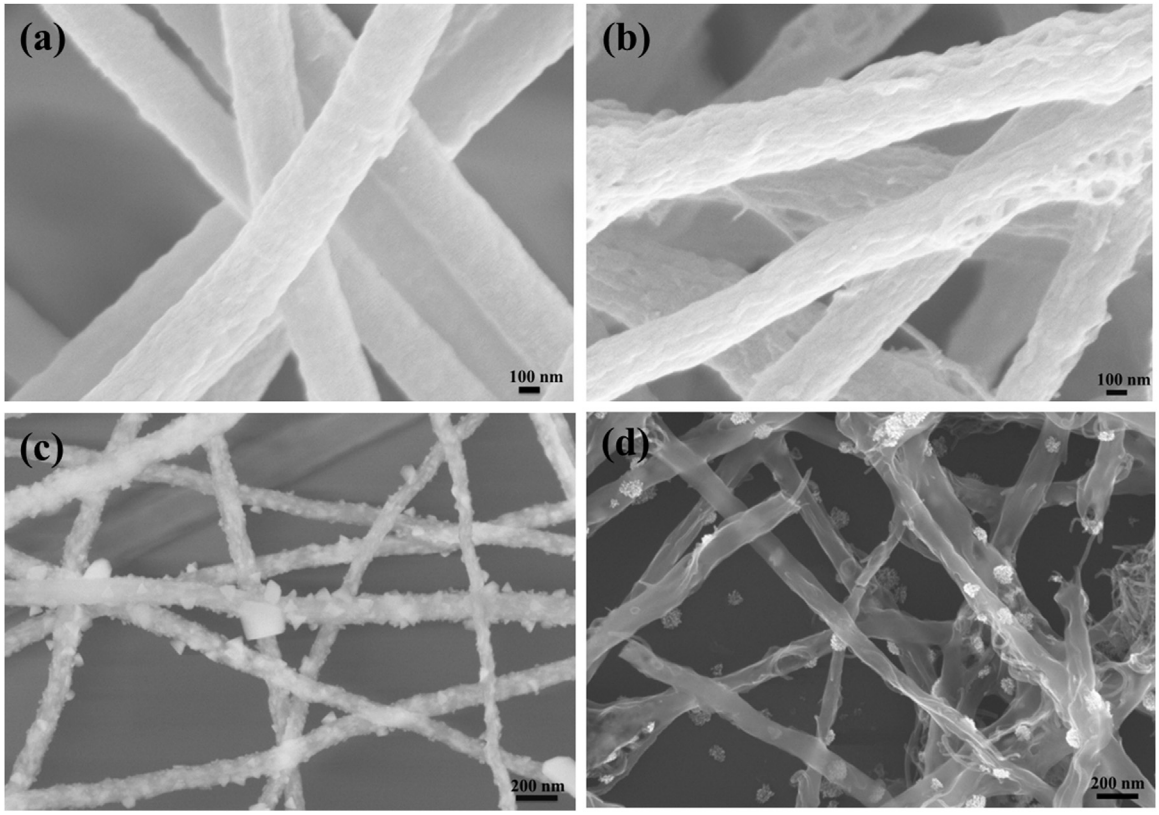

Fig. 1. FESEM image of (a) ZnO nanofiber before calcination (b) MWCNT-ZnO nano-fiber before calcination (c) ZnO nanofiber (ZnONF) after calcination (d) MWCNT-ZnO (MZnONF) after calcination.

optimized to 4 wt% to avoid electrostatic repulsion at higher conductivity and segregation at the grain boundaries at higher MWCNT concentration. When the applied electric field overcomes the surface tension of the viscous polymer solution, thin polymer jet is ejected and nanofibers were collected on the targeted silicon wafer. The collected nanofibers were further calcined at a critical temperature to obtain uniform MWCNT-ZnO nanofiber (MZnONF) after the decomposition of PAN polymer. The calcination temperature was optimized to avoid any decomposition of CNTs at higher temperature. After the calcination, the average diameters of nanofibers shrunk to 160–175 nm (Fig. 1c) in the case pure ZnO nanofibers and 185–200 nm in the case of MZnONF. The TEM image of MZnONF mat deposited on the copper grid is shown in Fig. 2a. A uniform distribution of MWCNTs is evident in the same and thus confirming the formation of the MWCNT-ZnO hybrid structure. Fig. 2a inset shows the focused TEM image of single MZnONF at higher magnification. The interface of the CNT and ZnO in MZnONF were observed from high resolution TEM (HRTEM) as shown in Fig. 2b and the inset figure shows the SEAD pattern of the MZnONF nanofiber.

The crystal phase formation and graphite existence of MZnONF were confirmed with XRD analysis. Fig. S1(a) shows the XRD data for MZnONF before the calcination. The peak shows at 16.9° corresponding to the (1 1 0) PAN reflection and the other peaks found at $2\theta = 26°$ and 43° correspond to (002) and (100) graphitic planes, respectively (McNally et al., 2005). It can be observed that no peak corresponding to ZnO is visible in the XRD pattern of nanofiber before calcination . However with the increase in the calcination temperature of nanofiber, the crystal planes corresponding to ZnO starts appearing in the XRD pattern. At 400 °C, the peak corresponding to the orthorhombic PAN (1 1 0) reflection vanishes. It can be ascribed to the degradation of PAN at 400 °C and complete transformation of MWCNT/PAN/ZnAc nanofiber to MWCNT-ZnO (MZnONF) nanofiber (Li et al., 2014). Fig. 2c shows the XRD pattern of MZnONF nanofiber calcined at 400 °C. The peaks found at 31.7°, 34.4°, 36.28°, 47.5°, 56.6°, 62.8°, 67.9° and 69.1° corresponding to (100), (002), (101), (102), (110), (103), (200), (112), and (201) respectively, of the ZnO wurtzite crystal structure (Mali et al., 2013). The other peaks position shows good agreement with those of graphite plane of MWCNTs, which indicates the structural intactness of MWCNTs. A further increase in calcination temperature up to 450 °C induces the decomposition of MWCNT and no peak was observed corresponding to graphite plane (Fig. S1(c)). Behler et al. (2006) observed the MWCNT damage at temperature above 430 °C. EDX analysis was carried out to confirm the presence of the wt% of carbon in MZnONF at different calcination temperatures (Fig. S2). It is important to note that the significant loss in wt% of carbon occur in a temperature range between 400 °C to 450 °C, which indicate the damages of the MWCNTs by oxidation. Hence, we selected the calcination temperature at 400 °C in order to avoid the decomposition of MWCNT. Fig. S3 shows the EDX spectra and mapping of MZnONF calcined at 400 °C, which, confirms presence of Zn, O_2 and C elements in MZnONF.

X-ray photoelectron spectroscopy was also used to characterize the chemical compositions on the nanofiber surface. XPS survey spectrum of MZnONF is shown in the Fig. S4(a). As expected, it contains carbon, oxygen and zinc elements. The core level C 1s spectrum of MZnONF is shown in Fig. S5(a). The peak observed at 284.5 eV and 285.5 eV attributed to the sp^2 carbon and defect containing sp^2 carbons respectively. The other weak peak located at 288.8 corresponding to carboxyl group (O=C–O) (Hemalatha et al., 2014; Jitianu et al., 2004). The peaks (Fig. S5(b)) at binding energy of 1021.5 and 1044.9 eV in pure ZnO nanofibers can be attributed to $Zn2p_{3/2}$ and $Zn2p_{1/2}$ respectively. However, a slight

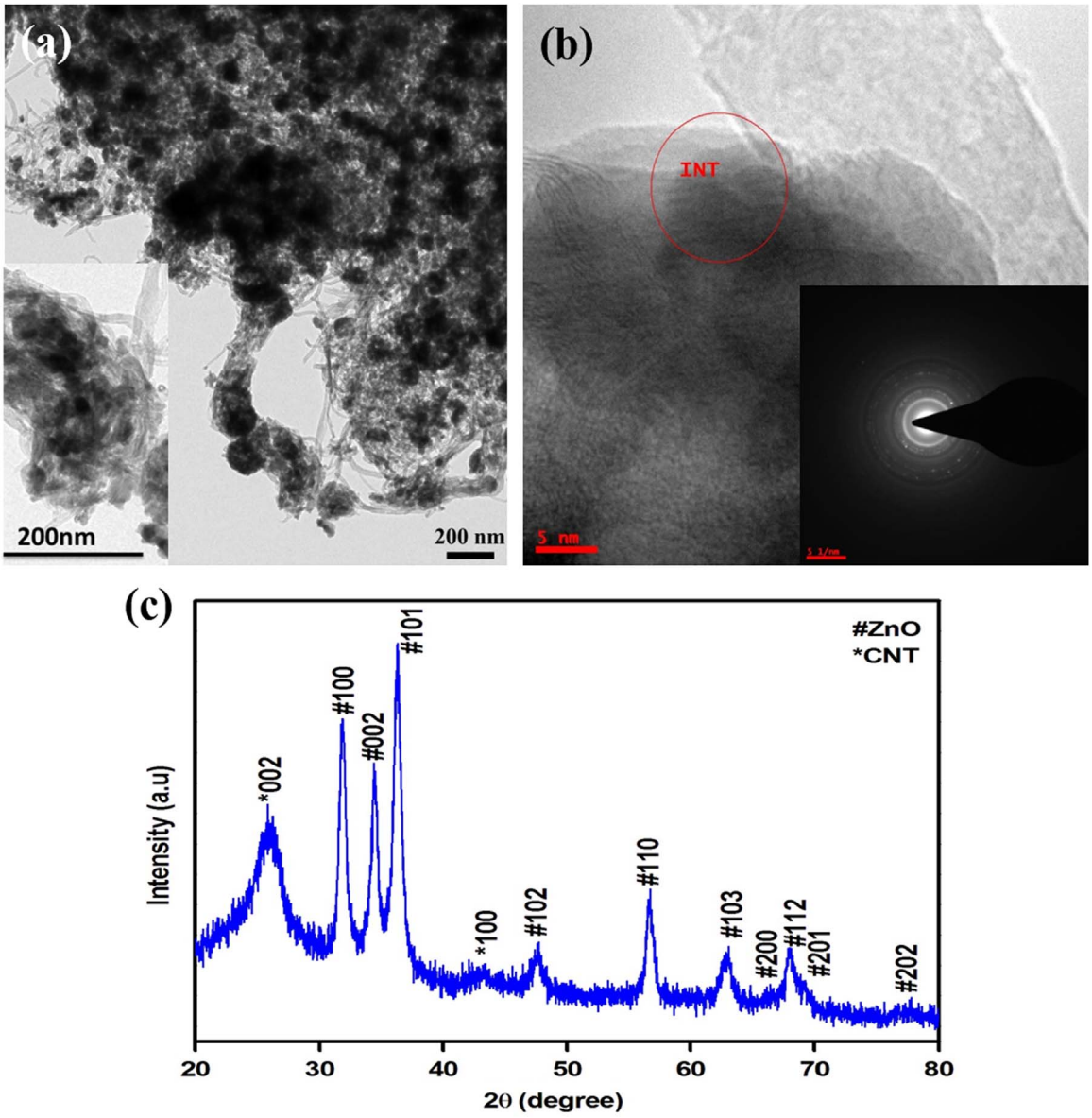

Fig. 2. TEM image of (a) MZnONF nanofiber (inset) single nanowire (b) HRTEM image of interface of ZnO and CNT in MZnONF nanofiber (Inset) SEAD pattern of MZnONF nanofiber (c) XRD analysis of MZnONF nanofiber.

shift to higher binding energy can be found for MZnONF compared with the pure ZnONF suggesting the formation of Zn–O–C bond between MWCNT and ZnO.

The FTIR spectrum of the ZnONF and MZnONFs are shown in Fig. S4(b). The peak observed at 530 cm^{-1} Zn–O bending and the weak peak found at 3360 cm^{-1} due to Zn-OH stretching of pure ZnO nanofiber. The characteristic peaks found near at 2830 and 2904 cm^{-1} attributed to the H–C stretch mode of COOH functionalized CNT-ZnO nanofiber (MZnONF) (Hemalatha et al., 2014). The bands in the region of 2500–3000 cm^{-1} due to the OH stretching mode arises from the carboxylic acid. The peak appeared near at 1750 cm^{-1} corresponding to the carboxylic group compared to the IR spectrum of pristine CNT (Jitianu et al., 2004; Salzmann et al., 2007).

Raman spectroscopy analysis has been carried out on MZnONFs for confirmation of the presence of MWCNT in MWCNT-ZnO nanofibers as shown in Fig. S4(c). The Raman spectra shows D band at about 1346 cm^{-1} and G band at 1578 cm^{-1} which is correspond to the E2g tangential stretching mode of an ordered graphitic structure and disordered carbon respectively. The downward shifting of the D and G band peak positions when compared to the functionalized MWCNT is due to the new bond formation between WMCNT and ZnO (Hirsch, 2002; Tan et al., 2007). The downward shifting of G′ band (2682 cm^{-1}) is because of the stretching of MWCNT (Ewsuk,2007). Interestingly, the ratio of D-band to G-band intensities of (I_D/I_G) of MZnONF is found to increase when compared to pristine MWCNT. The increase in I_D peak reveals the creation of defects in MWCNT due to the calcination of the nanofiber at higher temperature which, enables the defective carbons to be functionalized into carboxylic groups (–COOH) (Behler et al., 2006; Li et al., 2007). This can be utilized to functionalize the proteinsin to MZnONF surface through covalent binding (amide bond). Fig. S4(d) depicts the UV–vis absorption spectroscopy of ZnONF (red curve) and MZnONF (blue curve) respectively. The band gap of MZnONF nanofibers is calculated to be 3.01 eV as compared to the band gap of ZnONF nanofibers which is 3.28 eV. The narrowing of the band gap (Eg) is due to the formation of Zn–O–C bonds between ZnO and MWCNT in MZnONF (Nazir and Naqvi, 2013).

Please cite this article as: Paul, K.B., et al., (2016), http://dx.doi.org/10.1016/j.bios.2016.07.114

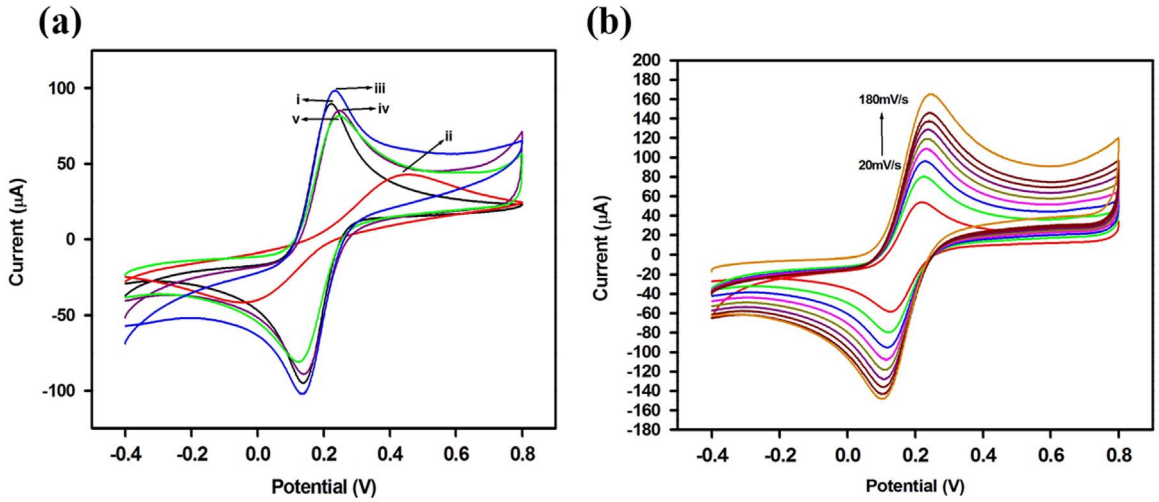

Fig. 3. Cyclic voltammetry (CV) curve of (a) bare GCE (curve i), ZnONF/GCE (curve ii), MZnONF/GCE (curve iii) Anti-CA125/MZnONF/GCE (curve iv), BSA/Anti-CA125/MZnONF/GCE (curve v)(b) Anti-CA125/MZnONF/GCE at different scan rate (20 mV/s–180 mV/s).

3.2. Electrochemical characterization

Cyclic voltammetry (CV) and differential pulse voltammetry (DPV) studies were conducted to investigate the electrochemical behavior of various modified electrodes. Fig. 3a illustrates the CV of stepwise modification of the prepared immune electrodes in a wide potential range of −0.4 to 0.8 V in the presence of 5.0 mM $[Fe(CN)_6]^{3-/4-}$ mediator. The peak to peak voltage (ΔE) for the ZnONF/GCE electrode (curve ii) is found to increase to 399 mV as compared to that of CZnONF/GCE electrode (99 mV, curve iii). The larger peak to peak difference and reduction in the current is due to the insulating character of ZnO nanofiber. After the incorporation of MWCNT, the MZnONF provides an alternative conducting path and that results in enhanced electron transfer kinetics as compared to that of pure ZnO nanofibers. Again, it is observed that the conjugation of Anti-CA125 (curve iv) and BSA (curve v) reduces electrochemical current due to the insulating nature of proteins which hinders the further electron transport compared to MZnONF/GCE electrode. Fig. 3b shows the electrochemical behavior of Anti-CA125/MZnONF/GCE immunoelectrode as a function of scan rate (20–180 mV/s). It is observed that the shift in both oxidation and reduction peak currents towards the higher and lower potential respectively with increasing scan rates. The linear variation of both anodic and cathodic peak current with the square root of the scan rate indicates that the reaction show a diffusion controlled process and follows the corresponding equations are as follows.

$$I_a = 1.13 \times 10^{-5}\,\mathrm{A(s/mV)}\left[scanrate(\mathrm{mV/s})\right]^{1/2} + 5.96 \times 10^{-6}\,\mathrm{A},\ R^2 = 0.994 \quad (1)$$

$$I_c = -1.010 \times 10^{-5}\,\mathrm{A(s/mV)}\left[scanrate(\mathrm{mV/s})\right]^{1/2} - 1.578 \times 10^{-5}\,\mathrm{A},\ R^2 = 0.996 \quad (2)$$

The diffusion co-efficient of various fabricated electrodes can be determined using Randle Sevick equation (Nazir and Naqvi, 2013),

$$I_p = 2.69 \times 10^5 n^{3/2} A D^{1/2} C v^{1/2} \quad (3)$$

where, I_p is the peak current of immunoelectrode, n is the number of electrons involved in electrochemical reaction, A is the electrode surface area (cm^2), D is the diffusion coefficient, C is the concentration of redox couple, F is the faraday's constant, υ is the scan rate (V/s) and T is the absolute temperature (K). The higher diffusion coefficient of MZnONF/GCE ($2.14\times10^{-11}\ cm^2\ s^{-1}$)electrode as compared to that of ZnONF/GCE electrode ($0.41\times10^{-11}\ cm^2\ s^{-1}$) indicates the enhanced conductivity in MWCNT incorporated ZnO nanofiber. However, the antibody immobilized MZnONF/GCE electrode shows the decreased diffusion coefficient ($1.474\times10^{-11}\ cm^2\ s^{-1}$) due to insulating character of BSA and anti-CA125 molecules. The surface concentration of the antibody immobilized immunoelectrode can be calculated using the Laviron's relation (Saleh et al., 2010).

$$I_p = n^2F^2\gamma A\upsilon(4RT)^{-1} \quad (4)$$

where, I_p is the peak current of immunoelectrode, n is the number of electrons transferred, A is the electrode surface area (cm^2), γ is the surface concentration, F is the Faraday's constant, υ is the scan rate (V/s), R is the universal gas constant and T is the absolute temperature (K). It is found that the surface concentration for the antibody immobilized MZnONF/GCE immunoelectrode (1.62×10^{-8} mol/cm^2) is higher compared to the corresponding value(8.04×10^{-9} mol/cm^2) obtained for the ZnONF/GCE immunoelectrode. The enhancement of surface concentration obtained for the MZnONF/GCE electrode indicates that MZnONF modified electrode increases the binding site for antibodies when compared to ZnONF modified electrode. The heterogeneous electron transfer rate k_s was estimated by using the following equation (Nazir and Naqvi, 2013),

$$k_s = 2.18[\beta DnFv/RT)^{1/2}\exp[(-\beta^2 nF/RT)(E_{pa}\_E_{pc})] \quad (5)$$

where, β is the electron transfer coefficient, D is the diffusion coefficient, n is the number of electrons transferred, υ is the scan rate and $E_{pa}\_E_{pc}$ is the peak separation. The heterogeneous electron transfer rate constant k_s for MZnONF was calculated to be 3.795×10^{-6} cm s^{-1}which is higher than that of the ZnONF (3.515×10^{-8} cm s^{-1}) indicating the fast electrons transfer at the MZnONF/GCE electrode surface. However, the electron transfer rate found to be reduced to 2.49×10^{-6} cm s^{-1} after the conjugation of BSA and anti- CA125 molecules.

Fig. S6 shows the DPV response of bare GCE (curve 1), MZnONF/GCE (curve 2), Anti-CA125 MZnONF/GCE (curve 3) and BSA/Anti-CA125/MZnONF/GCE (curve 4) electrodes. It is found that MZnONF/GCE electrode exhibits a peak current of 184.49 μA. After the conjugation of anti- CA 125 antibody and BSA molecules, the peak current reduced to 134.2 μA and 96.05 μA respectively. This is

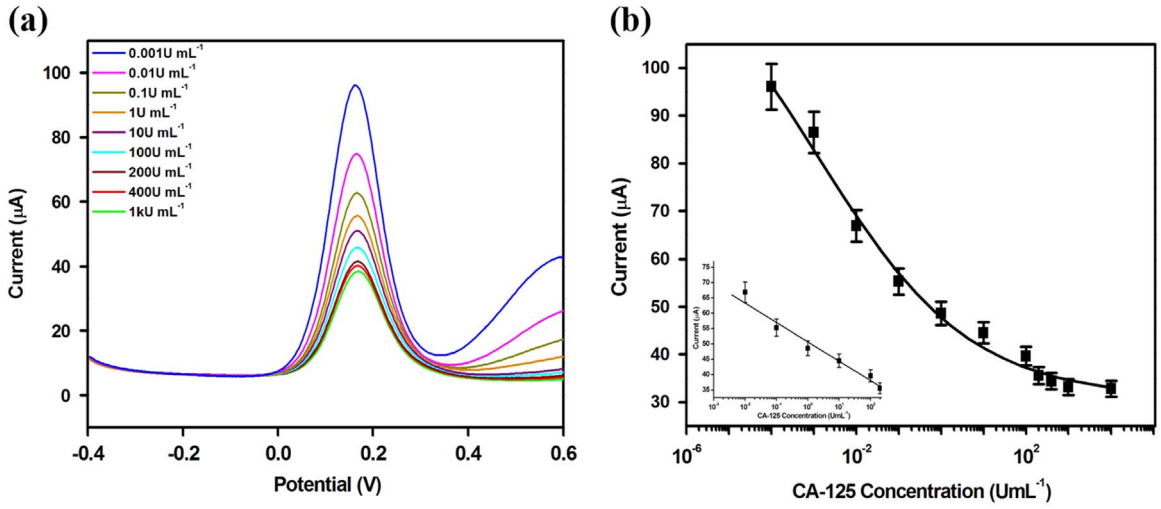

Fig. 4. (a) Differential pulse voltammetric (DPV) response of the BSA/Anti-CA125/MZnONF/GCE immunoelectrode as a function of CA125 concentration (b) Calibration curve of the biosensor using a logarithmic scale fitted to sigmoidal curve (inset) dynamic linear range of the curve.

attributed to the insulating nature of the biomolecules which hinders the electron transport towards the electrode. Prior to carrying out the electrochemical response studies of CA-125 antigen towards BSA/Anti-CA125/MZnONF/GCE, we have investigated the performance of the MZnONF/GCE electrode using Biotin-streptavidin interaction as model system. Biotin–hydrazide was covalently immobilized on the MZnONF/GCE electrode surface (using same protocol) for the detection of various concentrations of streptavidin (Fig. S7). The fabricated electrode exhibits wider detection range of streptavidin and should prove to be feasible for the detection of other biomarkers.

3.3. Electrochemical response studies

The electrochemical response characteristics of BSA/Anti-CA125/MZnONF/GCE immunoelectrodes have been studied using differential pulse voltammetry (DPV) technique as a function of CA125 concentration in 0.01 M PBS (pH 7.4) solution containing $[Fe(CN)_6]^{3-/4-}$ with an incubation time for 30 min .Fig. 4a shows the DPV response of immunoelectrode with the target CA125 antigen concentration over the range of 0.001to 1 kUmL^{-1}. The magnitude of the peak current decreased with the increasing target CA125 concentration. This can be attributed to the formation of immuno-complexes between CA125 and anti-CA125 antibodies that hinder the diffusion of the redox probe toward the electrode surface. Further it is observed that at higher concentration (after 1 kU/mL) of CA125 antigen, response current tends to saturate. The experiments were repeated three times for each concentration. A control experiment was conducted to investigate the electrochemical response of immunoelectrode towards the CA 125 antigen without using anti-CA 125 antibody (Fig. S8). However, no significant change in the current response was observed with respect to different concentration of CA 125. Even after 15 times of repeated cyclic voltammetry measurements, no obvious signal changes were observed (RSD=2.71%). This indicates that the change in electrochemical response current is likely to be due to the interaction between anti-CA 125 and CA 125 antigens. The calibration curve of DPV response current versus CA125 concentration is plotted for all the range and experimental data were fitted to a Rodbard's four Parameter logistic function describing a sigmoidal binding curve which follows Eq. (6) (Fig. 4b) (Warwick, 1996).

$$I(\mu A) = \frac{102.19 \times 10^{-4}}{1 + \left(\frac{\text{CA125concentration}\left(\text{UmL}^{-1}\right)}{0.00112} \right)^{\frac{1}{0.238}}} + 3.09 \times 10^{-5} \quad (6)$$

The limit of detection (LOD) can be calculated as,

$$LOD = EC_{50}\left(\frac{A_1 - A_2}{A_1 - A_2 - (3\sigma)} \right)^{1/P} \quad (7)$$

where, A1 is the minimum asymptote and A2 is the maximum asymptote, EC_{50} is the concentration corresponding to the 50% of the maximal signal change (inflection point), σ is the standard deviation of blank and P is the slope at the inflection point of the sigmoid curve. The limit of detection (LOD) for immunoelectrode is obtained to be 0.00113 UmL^{-1} using Eq. (7). The linear portion of the sigmoidal fitted curve is plotted as DPV response current versus the CA125 concentrations (Fig. 4b(Inset)), and the fabricated BSA/Anti-CA125/MZnONF/GCE bioelectrode exhibits a very high sensitivity of about 90.14 μA/(U/mL)/cm^2 (with R^2=0.97). The high sensitivity and ultra-low concentration detection may be attributed to the presence of MWCNT in MZnONF provides larger surface to volume ratio for protein immobilization and fast electron communication by proving short conducting path across the grain boundaries of ZnO . The electrochemical response characteristics of this BSA/anti-CA125/MZnONF/GCE based sensor for CA125 antigen detection are summarized in Table S1 along with those reported in the literature.

3.4. Interference, reproducibility, stability, and real sample analysis of the immunosensor

The effect of potential interferences on immunosensor is the key factor in fabrication of biosensor. The interference studies were performed using various interferents such as immunoglobulin G (IgG,10 ng/mL), bovine serum albumin (BSA,10 ng/mL), histidine-rich protein II (HRP2,10 ng/mL), creatinine (10 ng/mL) and mixture of the above interfering agents along with targeted 10 UmL^{-1} CA-125 antigen (Fig. 5a). The normalized peak current variation due to the interfering agents was less than 5% (with RSD=1.74%)as compared with the result obtained in the presence of 10 UmL^{-1} CA-125 only. This result clearly Indicate that the fabricated immunosensor possesses a good selectivity. The reproducibility of the immunosensor was evaluated by detecting

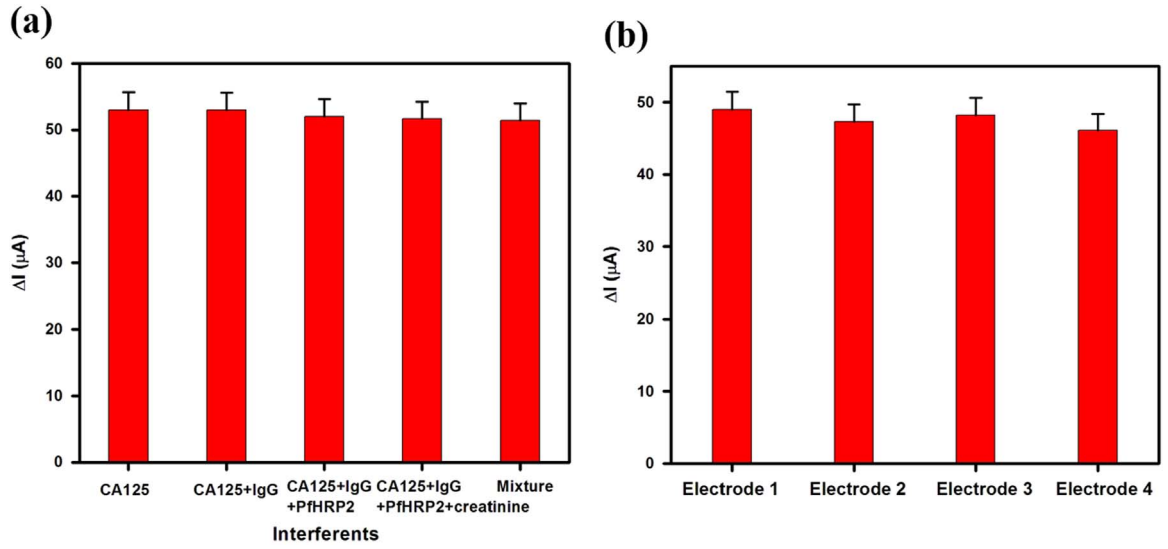

Fig. 5. (a) Interferents studies of BSA/Anti-CA125/MZnONF/GCE immunoelectrodes in presence of carcinoma antigen-125 with various concentration of other biomolecules (b) Reproducibility of immunoelectrodes.

Table 1
Recovery results of the carcinoma antigen-125 in human serum samples using proposed immunosensor.

Sample	Carcinoma Antigen −125 concentration (U/mL)		Recovery (%)	RSD, n=3 (%)
	Added	Found		
1	0.01	9.63×10^{-3}	96.3	3.07
2	0.1	9.94×10^{-2}	99.4	4.59
3	1	1.032	103.2	3.66
4	100	101.44	101.4	3.49
5	200	195.5	97.8	1.60

0.01 UmL^{-1} of CA125 with four prepared immunoelectrodes under similar conditions. The relative standard deviation (RSD) is 3.6% (n=4), indicating that the reproducibility of the proposed immunosensor was good (Fig. 5b). These immunosensors can be successfully regenerated by glycine-HCl (0.2 M, pH 2.5) solution for three minutes. The stability of the BSA/anti-CA125/MZnONF/GCE immunoelectrode was investigated by detecting the 0.01 UmL^{-1} at an interval of 7 days up to 3 weeks (Fig. S9). The immunosensor was stored at 4 °C, when not in use. It was observed that the immunosensor retained 94.1% of the initial value after storage for three weeks, clearly indicating that the immunosensor exhibits acceptable stability.

In order to demonstrate the practical application of the proposed immunosensor, the recoveries for different concentration of CA 125 proteins in human serum were detected. Different concentration of CA 125 were spiked in to diluted human serum samples and the concentration of detected CA 125 was calculated from the related calibration graph. The recovery was in the range of 96.3–103.2% with an RSD of 1.60–4.59% (Table 1). This results indicates that the good accuracy and potential application of the proposed immunosensor for real sample analysis.

4. Conclusion

In summary, MWCNT embedded ZnO nanofiber based immunosensor has been fabricated for the label free efficient detection of carcinoma-125 antigens. The MWCNT-ZnONF has been prepared through simple, low cost electrospinning technique and proteins (antibody) are conjugated to nanofiber via novel, one step surface functionalization process. The enhanced sensing performance have been achieved by combining the unique properties of ZnO and MWCNT and demonstrated using Biotin-streptavidin interaction as model system . The fabricated immune electrode (BSA/Ant-CA125/MZnONF/GCE) shows excellent sensitivity (90.14 μA/(U/mL)/cm^2) in the wider detection range of 1 mU/mL–1 kU/mL with a remarkable detection limit of 0.00113 U/mL. The results suggested the fabricated immunosensor showed good stability, reproducibility and acceptable selectivity. To the best of our knowledge, this is the first report on MWCNT-ZnO nanofiber based immunosensor explored for direct detection of carcinoma antigen-125. Efforts should be made to explore this MZnONF/GCE immunosensor platform for the detection of several important biomarkers towards developing point-of-care diagnostic devices.

Appendix A. Supporting information

Supplementary data associated with this article can be found in the online version at http://dx.doi.org/10.1016/j.bios.2016.07.114.

References

Ahmad, M., Pan, C., Luo, Z., Zhu, J., 2010a. J. Phys. Chem. C 114, 9308–9313.
Ahmad, M., Pan, C., Zhu, J., 2010b. J. Mater. Chem. 20, 7169–7174.
Ali, M.A., Mondal, K., Singh, C., Malhotra, B.D., Sharma, A., 2015. Nanoscale 7, 7234–7245.
Badgwell, D., Bast Jr., R.C., 2007. Dis. Markers 23, 397–410.
Batra, N., Tomar, M., Gupta, V., 2015. Biosens. Bioelectron. 67, 263–271.
Behler, K., Osswald, S., Ye, H., Dimovski, S., Gogotsi, Y., 2006. J. Nanopart. Res 8, 615–625.
Chen, S., Yuan, R., Chai, Y., Xu, Y., Min, L., Li, N., 2008. Sens. Actuators B Chem. 135, 236–244.
Ding, B., Wang, M., Wang, X., Yu, J., Sun, G., 2010. Mater. Today 13, 16–27.
Ewsuk, K., 2007. Characterization and Control of Interfaces for High Quality Advanced Materials II. John Wiley & Sons, New Jersey.
Fang, B., Zhang, C., Zhang, W., Wang, G., 2009. Electrochim. Acta 55, 178–182.
Felder, M., Kapur, A., Gonzalez-Bosquet, J., Horibata, S., Heintz, J., Albrecht, R., Fass, L., Kaur, J., Hu, K., Shojaei, H., 2014. Mol. Cancer 13, 1.
Gooding, J.J., 2005. Electrochim. Acta 50, 3049–3060.
Haghighi, B., Bozorgzadeh, S., 2011. Talanta 85, 2189–2193.
Hemalatha, K., Prakash, A., Guruprakash, K., Jayakumar, M., 2014. J. Mater. Chem. A 2, 1757–1766.
Hirsch, A., 2002. Angew. Chem. Int. Ed. 41, 1853–1859.
Hsu, P.-C., Wu, H., Carney, T.J., McDowell, M.T., Yang, Y., Garnett, E.C., Li, M., Hu, L., Cui, Y., 2012. ACS Nano 6, 5150–5156.

Jitianu, A., Cacciaguerra, T., Benoit, R., Delpeux, S., Beguin, F., Bonnamy, S., 2004. Carbon 42, 1147–1151.
Johari-Ahar, M., Rashidi, M., Barar, J., Aghaie, M., Mohammadnejad, D., Ramazani, A., Karami, P., Coukos, G., Omidi, Y., 2015. Nanoscale 7, 3768–3779.
Khanderi, J., Hoffmann, R.C., Gurlo, A., Schneider, J.J., 2009. J. Mater. Chem. 19, 5039–5046.
Lee, B.H., Song, M.Y., Jang, S.-Y., Jo, S.M., Kwak, S.-Y., Kim, D.Y., 2009. J. Phys. Chem. C 113, 21453–21457.
Li, Q., Li, Y., Zhang, X., Chikkannanavar, S.B., Zhao, Y., Dangelewicz, A.M., Zheng, L., Doorn, S.K., Jia, Q., Peterson, D.E., 2007. Adv. Mater. 19, 3358–3363.
Li, X., Zhang, H., Feng, C., Sun, Y., Ma, J., Wang, C., Lu, G., 2014. RSC Adv. 4, 27552–27555.
Liu, A., 2008. Biosens. Bioelectron. 24, 167–177.
Liu, H., Ma, H., Zhou, W., Liu, W., Jie, X., Li, X., 2012. Appl. Surf. Sci. 258, 1991–1994.
Mali, S.S., Kim, H., Jang, W.Y., Park, H.S., Patil, P.S., Hong, C.K., 2013a. ACS Sustain. Chem. Eng. 1, 1207–1213.
Matlock-Colangelo, L., Baeumner, A.J., 2012. Lab Chip 12, 2612–2620.
McNally, T., Pötschke, P., Halley, P., Murphy, M., Martin, D., Bell, S.E., Brennan, G.P., Bein, D., Lemoine, P., Quinn, J.P., 2005. Polymer 46, 8222–8232.
McQuarrie, S., Baum, R., Niesen, A., Madiyalakan, R., Korz, W., Sykes, T., Sykes, C., Hör, G., McEwan, A., Noujaim, A., 1997. Nucl. Med. Commun. 18, 878–886.
Morice, P., Brehier-Ollive, D., Rey, A., Atallah, D., Lhomme, C., Pautier, P., Pomel, C., Camatte, S., Duvillard, P., Castaigne, D., 2003. Ann. Oncol. 14, 74–77.
M. Nazir, I.I. Naqvi, 2013.
Nustad, K., Bast Jr., R., O'Brien, T., Nilsson, O., Seguin, P., Suresh, M., Saga, T., Nozawa, S., Børmer, O., De Bruijn, H., 1996. Tumor Biol. 17, 196–219.
Odaci, D., Telefoncu, A., Timur, S., 2008. Sens. Actuators B Chem. 132, 159–165.
Palanisamy, S., Cheemalapati, S., Chen, S.-M., 2012. Anal. Biochem. 429, 108–115.
Paul, K.B., Kumar, S., Tripathy, S., Vanjari, S.R.K., Singh, V., Singh, S.G., 2016. Biosens. Bioelectron. 80, 39–46.
Peng, N.-J., Liou, W.-S., Liu, R.-S., Hu, C., Tsay, D.-G., Liu, C.-B., 2011. Cancer Biother. Radiopharm. 26, 175–181.
Ravalli, A., Dos Santos, G.P., Ferroni, M., Faglia, G., Yamanaka, H., Marrazza, G., 2013. Sens. Actuators B Chem. 179, 194–200.
Saleh, T.A., Gondal, M., Drmosh, Q., 2010a. Nanotechnology 21, 495705.
Salzmann, C.G., Llewellyn, S.A., Tobias, G., Ward, M.A., Huh, Y., Green, M.L., 2007. Adv. Mater. 19, 883–887.
Samadi, M., Shivaee, H.A., Zanetti, M., Pourjavadi, A., Moshfegh, A., 2012. J. Mol. Catal. Chem. 359, 42–48.
Singh, N., Reza, K.K., Ali, M.A., Agrawal, V.V., Biradar, A., 2015. Biosens. Bioelectron. 68, 633–641.
Tak, M., Gupta, V., Tomar, M., 2013. J. Mater. Chem. B 1, 6392–6401.
Tak, M., Gupta, V., Tomar, M., 2014. Biosens. Bioelectron. 59, 200–207.
Tan, S., Sun, X., Yu, Z., Wu, P., Lo, G., Kwong, D., 2007. Appl. Phys. Lett. 91, 72101.
Vasudev, A., Kaushik, A., Bhansali, S., 2013. Biosens. Bioelectron. 39, 300–305.
Viswanathan, S., Rani, C., Ribeiro, S., Delerue-Matos, C., 2012. Biosens. Bioelectron. 33, 179–183.
Wang, Y., Yu, L., Wang, J., Lou, L., Du, W., Zhu, Z., Peng, H., Zhu, J., 2011a. J. Electroanal. Chem. 661, 8–12.
M. Warwick, 1996, Immunoass. Pract. Guide, pp. 150–170.
Wei, S., Yu, Y., Zhou, M., 2010a. Mater. Lett. 64, 2284–2286.
Wei, Y., Li, Y., Liu, X., Xian, Y., Shi, G., Jin, L., 2010b. Biosens. Bioelectron. 26, 275–278.
Wu, J., Fu, Z., Yan, F., Ju, H., 2007a. TrAC Trends Anal. Chem. 26, 679–688.
Wu, L., Yan, F., Ju, H., 2007b. J. Immunol. Methods 322, 12–19.
Zhang, C., Wang, G., Liu, M., Feng, Y., Zhang, Z., Fang, B., 2010a. Electrochim. Acta 55, 2835–2840.
Zhang, Y., Liu, Y., Li, X., Wang, Q.J., Xie, E., 2011. Nanotechnology 22, 415702.
Zhang, Z., Shao, C., Li, X., Wang, C., Zhang, M., Liu, Y., 2010b. ACS Appl. Mater. Interfaces 2, 2915–2923.
Zhao, M., Wang, X., Ning, L., Jia, J., Li, X., Cao, L., 2011. Sens. Actuators B Chem. 156, 588–592.
Zhao, Z., Chen, X., Tay, B., Chen, J., Han, Z., Khor, K.A., 2007. Biosens. Bioelectron. 23, 135–139.

Please cite this article as: Paul, K.B., et al., (2016), http://dx.doi.org/10.1016/j.bios.2016.07.114